PAPER

When finite-size effects dictate the growth dynamics on strained freestanding nanomembranes

Mourad Mezaguer, Nedjma Ouahioune and Jean-Noël Aqua [iD] *

We investigate the influence of strain-sharing and finite-size effects on the morphological instability of hetero-epitaxial nanomembranes made of a thin film on a thin freestanding substrate. We show that long-range elastic interactions enforce a strong dependence of the surface dynamics on geometry. The instability time-scale τ is found to diverge as $(e/H)^{-\alpha}$ with $\alpha = 4$ (respectively 8) in thin (resp. thick) membranes, where e (resp. H) is the substrate (resp. nanomembrane) thickness, revealing a huge inhibition of the dynamics as strain sharing decreases the level of strain on the surface. Conversely, τ vanishes as H^2 in thin nano-membranes, revealing a counter-intuitive strong acceleration of the instability in thin nanomembranes. Similarly, the instability length-scale displays a power-law dependence as $(e/H)^{-\beta}$, with $\beta = \alpha/4$ in both the thin and thick membrane limits. These results pave the way not only for experimental investigation, but also, for the dynamical control of the inescapable morphological evolution in epitaxial systems.

1 Introduction

A huge amount of research has been devoted in the past decade to investigate nanomembranes (NM) and apply them in innovative devices especially in flexible electronics.[1,2] They represent a credible alternative especially for group IV semiconductors to extend Moore's law and circumvent its collapse due to size reduction. Of special interest, NM allow strain-engineering of electronic properties, which is one of the most promising routes to bypass the physical limits of Si.[3–8] They are also characterized by easy shapeability and transferability that are a serious advantage for their integration in new micro-electronic devices. Different techniques are available for the production of crystalline NM on different kinds of support.[9–13] The resulting NM can be deformed and are attractive for flexible optoelectronics, photonics and nanoelectronics, *e.g.* in radiofrequency or thermally degradable devices, magnetotransport systems, micromechanical systems, infrared phototransistors and also for biological applications.[14–23]

We consider in the following a hetero-epitaxial nanomembrane where a thin crystalline film of thickness h is coherently deposited on a thin substrate of thickness e that is supposed to be freestanding and flat. The lattice mismatch between the film and substrate generates strain, and the long-range elastic field penetrates throughout the system, building an explicit dependence on geometry. First, strain sharing occurs between the film and substrate and is quantified by the ratio e/H

(with H the system thickness $H = e + h$). Second, any modulation of the surface with a lateral extension λ produces a field that extends also down to λ in the film and substrate, leading to a dependence on H (or more precisely on H/λ).[24] These two strain-sharing and finite-size effects introduce a new way to tune strain at will thanks to geometry. In addition, it is known that the strain thus produced may cause the morphological evolution of the surface when surface diffusion is active. This is basically described by the Asaro–Tiller–Grinfeld (ATG) instability[25,26] that is especially at work in SiGe systems at low strain[27] (as opposed to the nucleation occurring at higher strain[28]). We therefore revisit this instability to investigate the influence of finite-size effects and strain sharing on the dynamics of the growth of a film deposited on a nanomembrane substrate. We thence focus on the growth dynamics of the film, and not on equilibrium effects such as the ones for example that rationalize ordering of quantum dots on nanomembranes thanks to energetic considerations, see *e.g.* ref. 29–31.

In the following, we compute first the strain field generated in a hetero-epitaxial nanomembrane with free boundary conditions, corresponding to ultra-high vacuum conditions. We compute strain both in the flat film geometry and for a modulation with small slopes. This solution at linear order allows us to compute analytically the surface dynamics due to surface diffusion for a single harmonic. By Fourier decomposition, we then compute the surface evolution during annealing. We show that the dynamics is strongly affected by both finite-size and strain-sharing effects, with a possible dynamical inhibition or conversely strong acceleration of the morphological instability.

Sorbonne Université, CNRS, Institut des Nanosciences de Paris, INSP, UMR 7588, 4 Place Jussieu, 75005 Paris, France. E-mail: aqua@insp.jussieu.fr

The characteristic time and length scales are then shown to behave algebraically as a function of e/H and H.

2 Finite-size elasticity

We first turn to the computation of the elastic strain and energy in a hetero-epitaxial nanomembrane where the substrate is supposed to be flat and freestanding. It may correspond to experiments on a freestanding crystalline-sheet substrate or on a thin sheet with very weak interactions with its underlying substrate. We consider a thin film of thickness h on a thin substrate of thickness e, with $H = h + e$, the membrane thickness, see Fig. 1. The film surface is characterized by its free boundary at $z = H(\boldsymbol{r})$ where $\boldsymbol{r} = (x, y)$, while the substrate lower surface is located at $z = 0$. In isotropic elasticity, the displacement $\boldsymbol{e}$ and stress $\boldsymbol{\sigma}$ tensors are related by[32]

$$\boldsymbol{\sigma} = \frac{Y}{1+\nu}\left(e + \frac{\nu}{1-2\nu}\mathrm{Tr}[e]\,\mathbb{1}\right), \tag{1}$$

where Y and ν are the Young's modulus and Poisson's ratio of the film and substrate, supposed to be identical at the lowest order. When the interface is coherent, stress arises in the whole system from the lattice mismatch between the film and substrate, that is quantified by the misfit $m = 1 - a^{\mathrm{f}}/a^{\mathrm{s}}$, with $a^{\mathrm{f(s)}}$ the film (substrate) lattice parameter. Using the reference state defined with the substrate lattice parameter, the strain tensor is $e^{\alpha}_{pq} = \frac{1}{2}(\partial_q u^{\alpha}_p + \partial_p u^{\alpha}_q) - \eta^{\alpha}\delta_{pq}$, with $\eta^{\mathrm{s}} = 0$ in the substrate ($\alpha = $ s) and $\eta^{\mathrm{f}} = m$ in the film ($\alpha = $ f). Mechanical equilibrium enforces the local relationship

$$\boldsymbol{\nabla} \cdot \boldsymbol{\sigma} = 0, \tag{2}$$

but the strain state is fully determined by the boundary conditions. We assume that the substrate is freestanding, and that the nanomembrane is embedded in an ultra-high vacuum. As a consequence, both the substrate lower surface and the film upper are supposed to be free of stress (we also neglect surface-stress[33]). The surface boundary conditions are thence

$$\boldsymbol{\sigma} \cdot \boldsymbol{n}_z(z = 0) = 0 \tag{3a}$$

$$\boldsymbol{\sigma} \cdot \boldsymbol{n}(z = H) = 0 \tag{3b}$$

where $\boldsymbol{n}_z$ is the unit vector in the z direction, and $\boldsymbol{n}$, the unit vector normal to the film surface. Finally, when the interface is coherent, the displacement $\boldsymbol{u}$ and forces are continuous
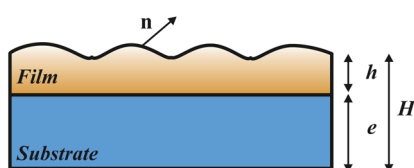

Fig. 1 Geometry of a nanomembrane with a film coherently deposited on a thin substrate of finite thickness.

$$\boldsymbol{u}(z = e^-) = \boldsymbol{u}(z = e^+), \tag{4a}$$

$$\boldsymbol{\sigma} \cdot \boldsymbol{n}_z(z = e^-) = \boldsymbol{\sigma} \cdot \boldsymbol{n}_z(z = e^+). \tag{4b}$$

The computation of the stress field may be done as a power-law expansion in the small-slope approximation where $|\nabla H| \ll 1$. Its results depend crucially on the level of stress in the zeroth-order flat-film geometry[34] where $H(\boldsymbol{r}) = H$ when the system is invariant by translation or rotation in the (x, y) plane. Hence, all the measurable properties such as forces, stress tensor and displacement gradients are independent of x and y, but not necessarily the displacement vector defined only up to an arbitrary reference state. In this geometry, the displacement vector $\boldsymbol{u}_0$ satisfies

$$\frac{\partial^2 \boldsymbol{u}_0}{\partial x^2} = \frac{\partial^2 \boldsymbol{u}_0}{\partial x \partial y} = \frac{\partial^2 \boldsymbol{u}_0}{\partial y^2} = 0. \tag{5}$$

Given the invariance of $\boldsymbol{\sigma}$ on x and y, Navier eqn (2) projected on the x direction leads to the fact that σ_{xz}, and thence e_{xz} and $\partial u_{0,x}/\partial x$, are constant both in the film and substrate. Similarly, the projection of (2) on the z-direction leads to a constant σ_{zz} and $\partial u_z/\partial z$ in the film and in the substrate, and to the same conclusion for $\partial u_{0,z}/\partial x$ and $\partial u_{0,z}/\partial y$ (after differentiation of σ_{zz} with respect to x). The general solution for the mechanical equilibrium accounting for the flat geometry is then

$$\boldsymbol{u}^{\alpha}_0 = \begin{pmatrix} a^{\alpha}_1 & a^{\alpha}_2 & a^{\alpha}_3 \\ a^{\alpha}_2 & a^{\alpha}_1 & a^{\alpha}_3 \\ a^{\alpha}_4 & a^{\alpha}_4 & a^{\alpha}_5 \end{pmatrix} \cdot \boldsymbol{R} + \boldsymbol{b}^{\alpha} \tag{6}$$

in the film and substrate ($\alpha = $ f or s), where $\boldsymbol{R} = (x, y, z)^T$ and choosing a reference state symmetric with respect to x and y. The stress-free surface boundary conditions (3a) and (3b) give $a^{\alpha}_4 = -a^{\alpha}_3$ while $a^{\alpha}_5 = -2\nu a^{\alpha}_1/(1 - \nu) + \eta^{\alpha}(1 + \nu)/(1 - \nu)$. We choose a reference state such as $b^{\mathrm{s}}_1 = 0$ in the substrate. The continuity relation (4a) leads to $a^{\mathrm{f}}_i = a^{\mathrm{s}}_i, b^{\mathrm{f}}_1 = 0$ while $b^{\mathrm{f}}_2 = -me(1 + \nu)/(1 - \nu)$. At this point, one is left with three unknowns, $a^{\mathrm{s}}_1, a^{\mathrm{s}}_2$ and a^{s}_3 that cannot be set by the remaining boundary condition (4b). Indeed, the Navier equation combined with the invariance along x and y leads to the invariance of $\boldsymbol{\sigma} \cdot \boldsymbol{n}_z$ along z. Thence, for a flat film where $\boldsymbol{n} = \boldsymbol{n}_z$, if (3a) and (3b) are satisfied, (4b) is automatically satisfied. To go further, we first set $a^{\mathrm{s}}_3 = 0$ thanks to an irrelevant rotation of the reference state around the z axis. Then, the solution for equilibrium is found by minimizing the total elastic energy. The latter reads per unit surface

$$E^{\mathrm{el}}_{\mathrm{tot}} = Y\left\{\frac{(e+h)}{1+\nu}a^{\mathrm{s}\,2}_2 + \frac{1}{1-\nu}\left[ea^{\mathrm{s}\,2}_1 + h\left(a^{\mathrm{s}}_1 - m\right)^2\right]\right\}, \tag{7}$$

in which a minimum is found for $a^{\mathrm{s}}_1 = mh/(e + h)$ and $a^{\mathrm{s}}_2 = 0$. Eventually, for a flat film, the displacement vector is at equilibrium

$$\boldsymbol{u}^{\alpha}_0 = \frac{mh}{e+h}\left(\boldsymbol{R} - \frac{1+\nu}{1-\nu}z\boldsymbol{n}_z\right) + \eta^{\alpha}\frac{1+\nu}{1-\nu}(z - e)\boldsymbol{n}_z. \tag{8}$$

In the limit of a semi-infinite substrate, eqn (8) leads to the known result $\boldsymbol{u}_{0,\infty}^{\alpha} = \dfrac{1+\nu}{1-\nu}\eta^{\alpha}(z-e)\boldsymbol{n}_z$, that vanishes in the substrate and displays the Poisson's dilatation in the film. In the opposite limit $e \to 0$, one finds the symmetric case $\boldsymbol{u}_{0,0}^{\alpha} = m\boldsymbol{R} - \dfrac{1+\nu}{1-\nu}(m-\eta^{\alpha})(z-e)\boldsymbol{n}_z$ where the film is fully relaxed while the substrate displays the Poisson's dilatation in the opposite direction. In between, the solution (8) quantifies the strain shared between the film and the substrate. Finally, the elastic energy density $\mathscr{E} = \dfrac{1}{2}\boldsymbol{\sigma}\cdot\boldsymbol{e}$ associated with (8) is in the film

$$\overline{\mathscr{E}}_0 = \mathscr{E}_0\left(\frac{e}{H}\right)^2 \quad \text{with} \quad \mathscr{E}_0 = \frac{Y}{1-\nu}m^2. \tag{9}$$

We now turn to the case where the film is corrugated and displays small slopes. Writing $H(\boldsymbol{r}) = H + h_1(\boldsymbol{r})$ with $H = \langle H(\boldsymbol{r})\rangle$, one may find the solution for the displacement vector as an expansion $\boldsymbol{u} = \boldsymbol{u}_0 + \boldsymbol{u}_1 + \dots$, supposing that h_1 (in fact $|\nabla h_1|$) is a small parameter. At equilibrium, $\boldsymbol{u}_1$ may be conveniently found in Fourier space in the x and y directions, with the result given in Table 1.

$$\begin{pmatrix} C_1 \\ C_3 \\ C_5 \end{pmatrix} = 2m(1+\nu)\frac{e}{H}\frac{1}{\sinh^2(kH)-(kH)^2} \times \dots \tag{11}$$

$$\dots \times \begin{pmatrix} ik_x[\sinh(kH) - kh\cosh(kH)]/k \\ ik_y[(\sinh(kH) - kh\cosh(kH))]/k \\ kH\sinh(kH) \end{pmatrix} h_1(\boldsymbol{k}). \tag{12}$$

Given this solution for the C_is and thence for $\boldsymbol{u}$ (given explicitly in Appendix), one can compute the elastic energy density on the film surface at $z = H(\boldsymbol{r})$, that reads $\mathscr{E} = \overline{\mathscr{E}}_0 + \mathscr{E}_1$ with $\overline{\mathscr{E}}_0$ given in (9) and

$$\mathscr{E}_1 = -2(1+\nu)\mathscr{E}_0\mathscr{A}_k(e,H)kh_1(\boldsymbol{k}), \tag{13}$$

where

$$\mathscr{A}_k(e,H) = \frac{1}{2}\left(\frac{e}{H}\right)^2\frac{\mathrm{sh}(2kH)-2kH}{\mathrm{sh}^2(kH)-(kH)^2}. \tag{14}$$

In the limit of a semi-infinite substrate (where $e \gg h$ and $kH \gg 1$), one finds $\mathscr{A}_k \to 1$ as expected.[35] Otherwise $\mathscr{A}_k$ describes the influence of strain-sharing and of finite-size effects on elasticity.

Table 1 General solution for the displacement vector in a nanomembrane

$$\boldsymbol{u}_1^{\alpha}(\boldsymbol{k},z) = \frac{\cosh(kz)}{4k}\begin{pmatrix} 4kC_1^{\alpha} + \dfrac{k_x^2 kz}{(1-\nu)k^2}C_2^{\alpha} + \dfrac{k_x k_y kz}{(1-\nu)k^2}C_4^{\alpha} + \dfrac{ik_x kz}{1-\nu}C_5^{\alpha} \\[2mm] \dfrac{k_x k_y kz}{(1-\nu)k^2}C_2^{\alpha} + 4kC_3^{\alpha} + \dfrac{k_y^2 kz}{(1-\nu)k^2}C_4^{\alpha} + \dfrac{ik_y kz}{(1-\nu)}C_5^{\alpha} \\[2mm] \dfrac{2ik_x kz}{1-2\nu}C_1^{\alpha} + \dfrac{2ik_y kz}{1-2\nu}C_3^{\alpha} + 4kC_5^{\alpha} - \dfrac{2kz}{1-2\nu}C_6^{\alpha} \end{pmatrix}$$

$$+\frac{\sinh(kz)}{4k}\begin{pmatrix} \dfrac{2k_x^2 z}{1-2\nu}C_1^{\alpha} + \dfrac{(3-4\nu)k_x^2 + 4(1-\nu)k_y^2}{(1-\nu)k^2}C_2^{\alpha} + \dfrac{2k_x k_y z}{1-2\nu}C_3^{\alpha} - \dfrac{k_x k_y}{(1-\nu)k^2}C_4^{\alpha} - \dfrac{ik_x}{1-\nu}C_5^{\alpha} + \dfrac{2ik_x z}{1-2\nu}C_6^{\alpha} \\[2mm] \dfrac{2k_x k_y z}{1-2\nu}C_1^{\alpha} - \dfrac{k_x k_y}{(1-\nu)k^2}C_2^{\alpha} + \dfrac{2k_y^2 z}{1-2\nu}C_3^{\alpha} + \dfrac{4(1-\nu)k_x^2 + (3-4\nu)k_y^2}{(1-\nu)k^2}C_4^{\alpha} - \dfrac{ik_y}{(1-\nu)}C_5^{\alpha} + \dfrac{2ik_y z}{(1-2\nu)}C_6^{\alpha} \\[2mm] -\dfrac{2ik_x}{1-2\nu}C_1^{\alpha} + \dfrac{ik_x z}{1-\nu}C_2^{\alpha} - \dfrac{2ik_y}{1-2\nu}C_3^{\alpha} + \dfrac{ik_y z}{1-\nu}C_4^{\alpha} - \dfrac{k^2 z}{1-\nu}C_5^{\alpha} - \dfrac{2(4\nu-3)}{1-2\nu}C_6^{\alpha} \end{pmatrix},$$

$$\tag{10}$$

We find there are six unknown C_i^{α}s both in the film and substrate, and, contrarily to the semi-infinite case, both e^{kz} and e^{-kz} terms, with the wavevector $\boldsymbol{k}$ and $k = |\boldsymbol{k}|$. The boundary conditions at the interface (4a) and (4b) give $C_i^{\mathrm{f}} = C_i^{\mathrm{s}} \equiv C_i$ (independent of the film or substrate) for $i = 1 \dots 6$, that lead to $\boldsymbol{u}_1^{\mathrm{f}} = \boldsymbol{u}_1^{\mathrm{s}}$, an identity resulting from the hypothesis of an identical film and substrate elastic constants.[†] The boundary condition (3a) gives $C_2 = ik_x C_5$, $C_4 = ik_y C_5$ and $C_6 = i\nu(k_x C_1 + k_y C_3)/(1-\nu)$. Eventually, the surface boundary condition (3b) gives

[†] This was also proven in the semi-infinite substrate case.

3 Dynamical evolution

3.1 Fourier analysis

The elastic stress may be relieved by the morphological change of the film free surface when surface diffusion is at work, as described by the Asaro–Tiller–Grinfeld instability.[25,26,36] This corresponds to experiments where the film free surface is in contact with vacuum so that the surface diffusion is activated, while the surface diffusion on the lower substrate surface is inhibited, e.g. by contact with porous materials, or occurs on a larger time scale. Mass conservation on the film surface

thence enforces the diffusion equation[37] $\partial h/\partial t = D\Delta_s\mu$ where D is the diffusion constant, and Δ_s, the surface Laplacian. The chemical potential μ is the sum of the elastic energy density on the surface $\mathscr{E}$ and of the capillary term $\gamma\kappa$, where γ is the surface energy (we neglect here the surface energy anisotropy[38]) and $\kappa = -(h_{xx} + h_{yy})$ is the surface local mean curvature. Given the solution (13), one finds that a modulation of wave-vector $\boldsymbol{k}$ evolves in the linear approximation as $h_1(\boldsymbol{k}, t) = e^{i\boldsymbol{k}\cdot\boldsymbol{r}+\sigma t}$ with

$$\sigma(\boldsymbol{k}, e, h) = \mathscr{A}_k(e, H)k^3 - k^4, \tag{15}$$

in units of the space and time scales $l_0 = \gamma/[2(1 + \nu)\mathscr{E}_0]$ and $t_0 = l_0{}^4/(D\gamma)$.

We plot in Fig. 2, the resulting growth rate as a function of k and e for different membrane thicknesses H. It is first noted that σ can be either strongly increased or lowered depending on finite-size effects (ruled by H) and strain sharing (ruled by e/H). To quantify this, we compute the maximum of σ for a given e and H, that occurs at (k_{max}, σ_{max}), see Fig. 3. We take as a reference, the infinite-substrate limit $\sigma_\infty(k) = k^3 - k^4$ for which $\sigma_{max}^\infty = 27/256 \simeq 0.105$ and $k_{max}^\infty = 3/4$ (this limit occurs when both $H \gg 1$ and $e/H \simeq 1$, i.e. $e \gg h$). This limit is already nearly achieved when $H = 10$ and when strain sharing vanishes ($e/H \simeq 1$). By decreasing the membrane thickness, one finds a ten-fold increase in σ_{max} for $H = 1$ without strain sharing ($\sigma_{max} \simeq 1.15$
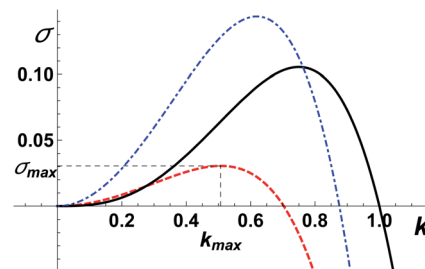

Fig. 3 (Dashed red line) Typical growth rate $\sigma(k, e, h)$ of the morphological instability as a function of its wavevector k when strain sharing is at work, for $e/H = 5/6$ and $H = 6$ in dimensionless units; (dot-dashed blue line) the same curve for $e/H = 1/2$ and $H = 2/3$; (black solid line) infinite substrate limit $\sigma_\infty(k)$.

when $e/H \simeq 1$) and a 10^3-fold increase for $H = 0.1$ ($\sigma_{max} \simeq 101$ when $e/H \simeq 1$). Hence, for a given e/H, the maximum growth rate increases with H, showing the *a priori* counter-intuitive influence of finite-size effects that enforce a faster relaxation for a thinner membrane. Conversely, for a given H, the growth rate significantly decreases when strain sharing occurs (i.e. when e/H decreases from 1). For $H = 10$, one finds respectively $\sigma_{max} = 0.105$, 9.5×10^{-4} and 1.0×10^{-6} for $e/H = 1$, 1/2 and 1/10. Similarly, for $H = 0.1$, one finds respectively $\sigma_{max} = 101$, 6.27 and 1.0×10^{-2} for $e/H = 1$, 1/2 and 1/10. Therefore, the stronger strain-sharing is (i.e. the lower e/H is), the slower the instability occurs, as the less strained the system is.

The second conclusion regarding $\sigma(k, e, H)$ is the variation of the maximum wavelength k_{max} as a function of finite-size and strain-sharing effects. We find, see Fig. 2, that for a given H, k_{max} decreases when strain-sharing increases (i.e. when e/H decreases) while, for a given e/H, k_{max} increases when finite-size effects increase (i.e. when H decreases). Numerically, we find for $H = 10$, respectively $k_{max} = 0.75$, 0.19 and 0.032 for $e/H = 1$, 1/2 and 1/10, while for $H = 0.1$, $k_{max} = 3.18$, 1.58 and 0.32 for $e/H = 1$, 1/2 and 1/10. The decreases of k_{max} with strain-sharing corroborate the fact that the film is globally less strained in this case. Conversely, the increase in k_{max} with finite-size effects is consistent with the increase in σ, signaling the increase in the surface strain in this case. Globally, even if the variation of k_{max} with e/H and H is quantitatively less pronounced than for σ_{max}, it is nonetheless significant and leads to variations that are expected to be important in experimental systems.

We note that for given strain-sharing and finite-size effects, the growth rate eqn (15) always displays a positive maximum so that the morphological instability should always occur (we neglect here the influence of wetting effects that can lead to the existence of a critical thickness,[35] in order to focus solely on the influence of strain-sharing and finite-size effects). Indeed, for given e/H and H, we find at low-k $\sigma(k, e, H) = 2e^2k^2/H^3 + \mathcal{O}(k^4)$,‡ while $\sigma(k, e, H) \approx -k^4$ at large k.§ Another interesting limit is the thin-membrane limit (when
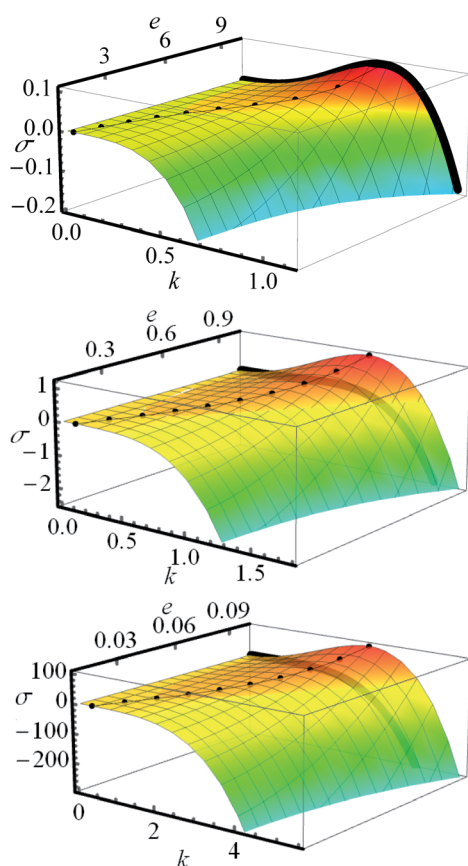

Fig. 2 Growth rate $\sigma(k, e, H)$ for $H = 10$ (top), $H = 1$ (middle) and $H = 0.1$ (bottom). The black thick solid line represents the reference $\sigma_\infty(k)$ corresponding to the semi-infinite substrate limit. The dots locate the maximum value (k_{max}, σ_{max}) of $\sigma(k, e, H)$ for given e and H.

‡ Note that the $k \to 0$ and $H \to \infty$ limits do not commute.
§ Subsequently, there exists k_+ such as $\sigma < 0$ for $k > k_+$, and the instability will occur only if no lateral finite-size effect occurs, i.e. only if $L > 2\pi/k_+$.

$H \ll 1$), where $\sigma(k, e, H) \approx \dfrac{e^4}{H^6}(2\tilde{k}^2 - \tilde{k}^4)$ with $\tilde{k} = k/k_t$ and $k_t = e/H^{3/2}$. When both e and H are of order ε, k_{max} diverges as $1/\sqrt{\varepsilon}$ while σ_{max} behaves as $1/\varepsilon^2$.

3.2 Real-space analysis

We now investigate an evolution that shows experimental systems where the ATG instability is at work, with the deposition of a film of a given thickness, followed by instability during a subsequent annealing. The initial condition is a film with a given thickness h on top of a thin substrate of thickness e, with an additional surface roughness on the film free surface. The latter stands for the deposition noise and thermal fluctuations, that is described here by an initial white noise with an amplitude of one monolayer. We then study surface diffusion during annealing. In this case, the surface is not characterized by a unique wave-vector, but may be decomposed as the sum of different Fourier modes with equal amplitude at $t = 0$ (describing a white noise). We consider only the linear regime of the surface diffusion equation (that is relevant in the small-slope approximation) where elasticity is given at first order in h by eqn (13). Hence, the different Fourier modes evolve independently following eqn (15), starting with equal amplitude, and evolving with different growth rates. We expect the fastest growing mode k_{max} to mainly rule the long-time behavior,[39] nevertheless within a time-scale where the linear regime applies, i.e. when the surface slope remains small.

The resulting typical evolution on top of a membrane is shown in Fig. 4. We characterize the surface geometry with the length-scale λ that can be related to the average wave-vector

$$\langle k \rangle = \frac{\sum_{k} |\boldsymbol{k}||\hat{h}(\boldsymbol{k})|^2}{\sum_{k} |\hat{h}(\boldsymbol{k})|^2}, \qquad (16)$$

(where the summation runs over the different Fourier modes), thanks to $\lambda = 2\pi/\langle k \rangle$. On the other hand, the dynamical evolution may be associated with a characteristic time τ, defined through the surface roughness $w(t) = \sqrt{\langle (h(\boldsymbol{r}, t) - h)^2 \rangle}$, by $w(t = \tau) = e w(t = 0)$. This time-scale rules the initial exponential increase in the surface roughness in the linear regime. In addition, these scales can be compared to the scales associated with the fastest growing mode k_{max}, $\lambda_{max} = 2\pi/k_{max}$ and $\tau_{max} = \alpha_N/\sigma_{max}$ where $\alpha_N = 1 + \frac{1}{2}\ln(N)$ accounts for the initial random noise uniformly distributed on N Fourier modes.

We plot in Fig. 5 and 6, the resulting characteristic scales for $H = 100$, 1 and 0.1. It is noteworthy that the typical time scale τ displays huge variations as a function of strain sharing and finite-size effects. For a given H, it shows a 10^4 (respectively 10^2) increase when e/H decreases from 1 to 0.4 for $H = 100$ (resp. 0.1), describing a strong slowdown of the instability evolution. This sensitivity is naturally related to the decrease in the global strain with strain-sharing, as described above for the growth rate σ. But we also find that τ decreases strongly when H decreases for a given e/H: we find e.g. a decrease from 30 down to 0.012 in between $H = 100$ and 0.1 for $e/H = 1$. This reveals the counter-intuitive result of these finite-effects, coherently related to their influence on the growth rate σ: a thinner membrane leads to a much faster surface dynamics, and the acceleration of the instability. Similarly, the typical wave-length of the instability is also ruled by strain-sharing and finite-size effects, but with a lower amplitude, see Fig. 6. The increase in λ when e/H decreases is again related to the decrease in the global strain but with a factor at most around 3 to 4, while its decrease when H decreases is also related to the counter-intuitive finite-size effects. In addition, we find that the resulting length and time scales λ and τ are very well approximated by λ_{max} and τ_{max}, showing that the fastest growing mode is quickly driving the surface dynamics. It is nonetheless not a perfect approximation,
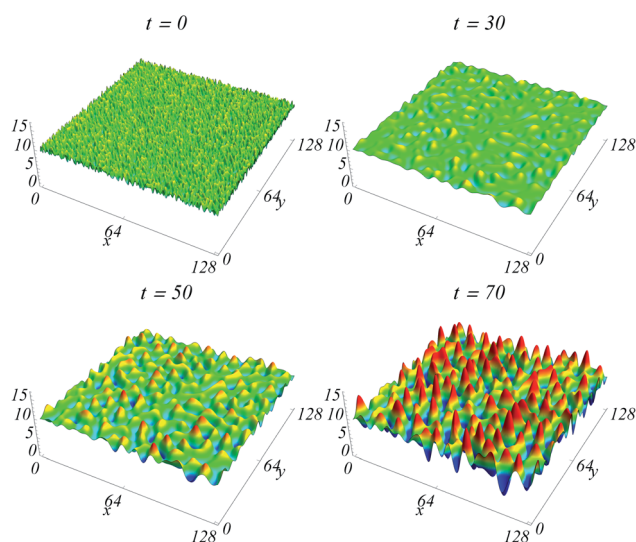

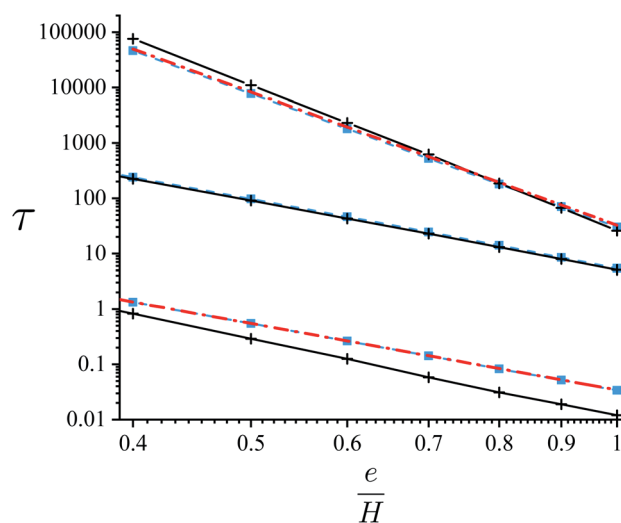**Fig. 4** Evolution of the film surface $h(x, y, t)$ for $H = 10$ and $e/H = 0.9$.

Fig. 5 Characteristic time-scale τ (black solid line) as a function of the strain-sharing ratio e/H and numerical estimate (dashed-blue line) for (top curve) $H = 100$, (middle) $H = 1$ and (bottom) $H = 0.1$. For the top and bottom curves, analytical approximation τ_{max} (dot-dashed red line) respectively for $H \gg 1$ and $H \ll 1$.
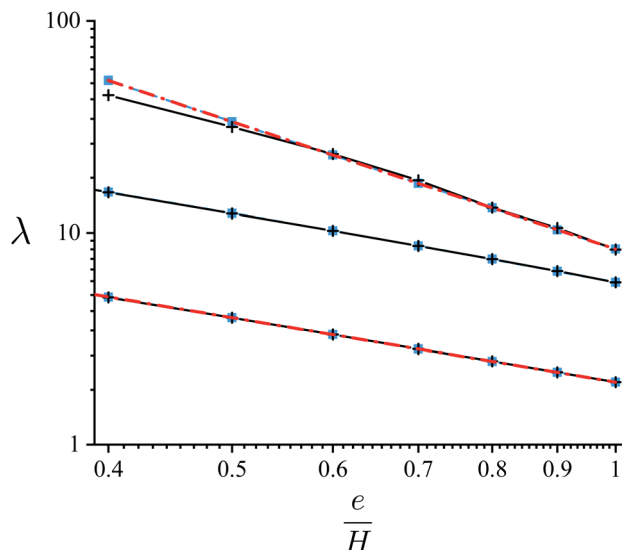
Fig. 6 Characteristic length-scale λ (black solid line) for large time t (nevertheless within the small-slope approximation) as a function of the strain-sharing ratio e/H and numerical estimate (dashed-blue line) for (top curve) $H = 100$, (middle) $H = 1$ and (bottom) $H = 0.1$. For the top and bottom curves, analytical approximation τ_{max} (dot-dashed red line) respectively for $H \gg 1$ and $H \ll 1$.

especially for τ and at low thickness H where the maximum of $\sigma(k)$ is less sharp.

To get some analytical insights on these evolutions, we find that the previous results can be well approximated in some limits, see Fig. 5 and 6. When finite-size effects vanish, i.e. for $H \gg 1$, one finds

$$\sigma^{H \gg 1}(k, e, H) \approx \left(\frac{e}{H}\right)^2 k^3 - k^4, \tag{17}$$

that can be maximized, giving the approximate

$$\tau_{max}^{H \gg 1} \approx \frac{256}{27}\alpha_N\left(\frac{e}{H}\right)^{-8}, \tag{18a}$$

$$\lambda_{max}^{H \gg 1} \approx \frac{8\pi}{3}\left(\frac{e}{H}\right)^{-2}. \tag{18b}$$

These approximations are plotted in Fig. 5 and 6 and do indeed perfectly capture the numerical estimate of τ_{max} and λ_{max}, and approximate well the global time and length scales τ and λ. In the other limit of strong finite-size effects, i.e. for $H \ll 1$, we find the Laurent series

$$\sigma^{H \ll 1}(k, e, H) \approx \frac{2}{H}\left(\frac{e}{H}\right)^2 k^2 - k^4, \tag{19}$$

leading to the approximates

$$\tau_{max}^{H \ll 1} = \alpha_N H^2\left(\frac{e}{H}\right)^{-4}, \tag{20a}$$

$$\lambda_{max}^{H \ll 1} = 2\pi\sqrt{H}\left(\frac{e}{H}\right)^{-1}, \tag{20b}$$

that again approximate well both the numerical estimates τ_{max} and λ_{max}, and more importantly the global values τ and λ, see Fig. 5 and 6. Hence, these power-laws characterize well the strong variations of τ and λ as a function of strain-sharing and finite-size effects. Finally, we also plot the results of the intermediate case for $H = 1$ in Fig. 5 and 6, that is characterized here by $\tau^{H=1} = 5.6(e/H)^{-4.0}$ while $\lambda^{H=1} \approx 6.0(e/H)^{-1.0}$ with exponents close to the $H \ll 1$ limit. Note that in all cases, as t_0 scales as l_0^4, it is natural to find here that the dependence of τ on e/H is as λ^4.

4   Conclusion

As a conclusion, we have investigated the influence of strain-sharing and finite-size effects on the morphological instability at work in strained nano-membranes. We have shown that geometric parameters can tune the nanomembrane surface dynamics and rule either its strong acceleration in thin nano-membranes, or its strong inhibition when strain is significantly shared. This theoretical study may serve as a guide to rationalize and control experiments on such systems. One of its natural extension concerns the study of sandwiched film/substrate/film geometries where corrugations grow on both sides of the NM. The initial linear evolution in such geometries should correspond to the results of the present analysis, while correlations between the NM both sides are expected to arise at non-linear order and are currently under investigation.

5   Appendix

The full solution for the displacement vector at first order in the surface slope is eventually

$$\boldsymbol{u}_1(\boldsymbol{k}, z) = m\frac{1 + \nu}{1 - \nu}\frac{e}{H}\frac{1}{1 + 2(kH)^2 - \cosh(2Hk)}\times$$
$$\dots \times \frac{\mathbf{D}(\boldsymbol{k}, z)}{k}h_1(\boldsymbol{k}) \tag{21}$$

with

$$D_x = i2k_x\{k\sinh(kz) \times \dots \times [((2\nu - 1)H - z)\sinh(kH) + kHz\cosh(kH)] - \cosh(kz)[(k^2Hz - 2(\nu - 1))\sinh(kH) + 2(\nu - 1)kH\cosh(kH)]\} \tag{22}$$

and a symmetric definition for D_y, while

$$D_z = -k\{\sinh(kH) \times \dots \times [\sinh(kz)(kz - k^2Hz - 2(\nu - 1)) - 2\cosh(kz)(kz - 2(\nu - 1)kH)] + 2kH\cosh(kH)[(2\nu - 1)\sinh(kz) + kz\cosh(kz)]\} \tag{23}$$

Conflicts of interest

There are no conflicts to declare.

Acknowledgements

References

1 Q. Guo, Z. Di, M. G. Lagally and Y. Mei, *Mater. Sci. Eng., R*, 2018, **128**, 1, ISSN 0927-796X.

2 G. Huang and Y. Mei, *Small*, 2018, **14**, 1703665.

3 M. Huang, C. Boone, M. Roberts, D. E. Savage, M. G. Lagally, N. Shaji, H. Qin, R. Blick, J. A. Nairn and F. Liu, *Adv. Mater.*, 2005, **17**, 2860, ISSN 1521-4095.

4 L. Zhang, E. Ruh, D. Grützmacher, L. Dong, D. J. Bell, B. J. Nelson and C. Schönenberger, *Nano Lett.*, 2006, **6**, 1311.

5 D. Y. Khang, H. Jiang, Y. Huang and J. A. Rogers, *Science*, 2006, **311**, 208.

6 A. Malachias, Y. Mei, R. K. Annabattula, C. Deneke, P. R. Onck and O. G. Schmidt, *ACS Nano*, 2008, **2**, 1715.

7 D. M. Paskiewicz, B. Tanto, D. E. Savage and M. G. Lagally, *ACS Nano*, 2011, **5**, 5814, DOI: 10.1021/nn201547k.

8 J. N. Aqua, L. Favre, A. Ronda, A. Benkouider and I. Berbezier, *Cryst. Growth Des.*, 2015, **15**, 3399, DOI: 10.1021/acs.cgd.5b00485.

9 C. Xu, X. Wu, G. Huang and Y. Mei, *Adv. Mater. Technol.*, 2019, **4**, 1800486.

10 S. A. Scott and M. G. Lagally, *J. Phys. D: Appl. Phys.*, 2007, **40**, R75, http://stacks.iop.org/0022-3727/40/i=4/a=R01.

11 J. A. Rogers, M. G. Lagally and R. G. Nuzzo, *Nature*, 2011, **477**, 45, DOI: 10.1038/nature10381.

12 I. Berbezier, J. N. Aqua, M. Aouassa, L. Favre, S. Escoubas, A. Gouyé and A. Ronda, *Phys. Rev. B: Condens. Matter Mater. Phys.*, 2014, **90**, 035315, DOI: 10.1103/PhysRevB.90.035315.

13 T. David, J. Aqua, K. Liu, L. Favre, A. Ronda, M. Abbarchi, J. Claude and I. Berbezier, *Sci. Rep.*, 2018, **8**, 2891, https://www.nature.com/articles/s41598-018-21299-9.

14 A. Ghaffari, A. Hosseini, X. Xu, D. Kwong, H. Subbaraman and R. T. Chen, *Opt. Express*, 2010, **18**, 20086.

15 J. Viventi, D. H. Kim, L. Vigeland, E. S. Frechette, J. A. Blanco, Y. S. Kim, A. E. Avrin, V. R. Tiruvadi, S. W. Hwang, A. C. Vanleer, D. F. Wulsin, K. Davis, C. E. Gelber, L. Palmer, J. Van der Spiegel, J. Wu, J. Xiao, Y. Huang, D. Contreras, J. A. Rogers and B. Litt, *Nat. Neurosci.*, 2011, **14**, 1599, DOI: 10.1038/nn.2973.

16 M. Ying, A. P. Bonifas, N. Lu, Y. Su, R. Li, H. Cheng, A. Ameen, Y. Huang and J. A. Rogers, *Nanotechnology*, 2012, **23**, 344004, http://stacks.iop.org/0957-4484/23/i=34/a=344004.

17 H. Fang, H. A. Bechtel, E. Plis, M. C. Martin, S. Krishna, E. Yablonovitch and A. Javey, *Proc. Natl. Acad. Sci. U. S. A.*, 2013, **110**, 11688, ISSN 0027-8424.

18 H. Zhou, J. H. Seo, D. M. Paskiewicz, Y. Zhu, G. K. Celler, P. M. Voyles, W. Zhou, M. G. Lagally and Z. Ma, *Sci. Rep.*, 2013, **3**, 1291.

19 J. S. Vorobyova, A. B. Vorob'ev, V. Y. Prinz, A. I. Toropov and D. K. Maude, *Nano Lett.*, 2015, **15**, 1673.

20 G. Li, E. Song, G. Huang, Q. Guo, F. Ma, B. Zhou and Y. Mei, *Adv. Funct. Mater.*, 2018, **28**, 1801448.

21 R. Pan, Q. Guo, J. Cao, G. Huang, Y. Wang, Y. Qin, Z. Tian, Z. An, Z. Di and Y. Mei, *Nanoscale*, 2019, **11**(36), 16844, DOI: 10.1039/C9NR05189A.

22 M. Vutukuru, J. W. Christopher, C. Pollock, D. J. Bishop and A. K. Swan, *J. Microelectromech. Syst.*, 2019, **28**, 550.

23 B. L. T. Rosa, C. A. Parra-Murillo, T. Chagas, A. J. Garcia Junior, P. S. S. Guimarães, C. Deneke, R. Magalhães-Paniago and A. Malachias, *ACS Appl. Nano Mater.*, 2019, **2**, 4655.

24 J. N. Aqua and X. Xu, *Surf. Sci.*, 2015, **639**, 20, http://www.sciencedirect.com/science/article/pii/S0039602815001016.

25 R. J. Asaro and W. A. Tiller, *Metall. Trans.*, 1972, **3**, 1789.

26 M. A. Grinfeld, *Sov. Phys. Dokl.*, 1986, **31**, 831.

27 K. Liu, I. Berbezier, T. David, L. Favre, A. Ronda, M. Abbarchi, P. W. Voorhees and J. N. Aqua, *Phys. Rev. Mater.*, 2017, **1**(5), 053402, DOI: 10.1103/PhysRevMaterials.1.053402.

28 K. Liu, I. Berbezier, L. Favre, A. Ronda, M. Abbarchi, P. Donnadieu, P. W. Voorhees and J. N. Aqua, *Nanoscale*, 2019, **11**, 7798–7804.

29 M. Huang, P. Rugheimer, M. G. Lagally and F. Liu, *Phys. Rev. B: Condens. Matter Mater. Phys.*, 2005, **72**, 085450, DOI: 10.1103/PhysRevB.72.085450.

30 H. J. Kim-Lee, D. E. Savage, C. S. Ritz, M. G. Lagally and K. T. Turner, *Phys. Rev. Lett.*, 2009, **102**(22), 226103, DOI: 10.1103/PhysRevLett.102.226103.

31 G. Vastola, V. B. Shenoy and Y. W. Zhang, *ACS Nano*, 2012, **6**, 3377, DOI: 10.1021/nn3003983.

32 L. Landau and E. Lifchitz, *Theory of Elasticity*, USSR Academy of Sciences, Moscow, USSR, 1986.

33 M. S. Levine, A. A. Golovin, S. H. Davis and P. W. Voorhees, *Phys. Rev. B: Condens. Matter Mater. Phys.*, 2007, **75**, 205312, DOI: 10.1103/PhysRevB.75.205312.

34 K. Liu, I. Berbezier, L. Favre, A. Ronda, T. David, M. Abbarchi, P. Gaillard, T. Frisch, B. Croset and J. N. Aqua, *Phys. Rev. Mater.*, 2019, **3**, 023403.

35 J. N. Aqua, T. Frisch and A. Verga, *Phys. Rev. B: Condens. Matter Mater. Phys.*, 2007, **76**, 165319, DOI: 10.1103/PhysRevB.76.165319.

36 B. J. Spencer, P. W. Voorhees and S. H. Davies, *J. Appl. Phys.*, 1993, **73**, 4955.

37 B. J. Spencer, P. W. Voorhees and S. H. Davis, *Phys. Rev. Lett.*, 1991, **67**, 3696, DOI: 10.1103/PhysRevLett.67.3696.

38 J. N. Aqua, A. Gouyé, T. Auphan, T. Frisch, A. Ronda and I. Berbezier, *Appl. Phys. Lett.*, 2011, **98**, 161909, DOI: 10.1063/1.3576916.

39 X. Xu, J. N. Aqua and T. Frisch, *J. Phys.: Condens. Matter*, 2012, **24**, 045002, http://stacks.iop.org/0953-8984/24/i=4/a=045002.